DIRECT NUMERICAL SIMULATION OF TURBULENT FLOW OVER A COMPLIANT SURFACE

Takahide Endo
Division of Computer and Information
The Institute of Physical and Chemical Research
2-1, Hirosawa, Wako-shi, Saitama, 351-0198, Japan
endo@postman.riken.go.jp

Ryutaro Himeno
Division of Computer and Information
The Institute of Physical and Chemical Research
2-1, Hirosawa, Wako-shi, Saitama, 351-0198, Japan
himeno@postman.riken.go.jp

ABSTRACT

Direct numerical simulation of turbulent channel flow with a compliant surface is made to evaluate the drag reduction effect. It is found that a slight drag reduction is observed with compliant surface. From this fact, it is shown that the drag reduction is possible by a compliant surface which is deformed passively by wall pressure fluctuation. Small wall displacement and velocity are observed in the present study, however, large scale of pressure field becomes dominant. The typical shape of the displacement of the compliant surface is a wave which is almost homogeneous in the spanwise direction.

INTRODUCTION

From the view point of saving power and protecting the environment, it is strongly desired to develop efficient turbulence control techniques for drag reduction and heat transfer augmentation. Creatures living in the water have developed an efficient turbulent control techniques in their unique evolutions. Typical examples are sharks. Scale of a shark has grooves in the streamwise direction, and a riblet surface is made after it. Walsh (1982) progressed a series of experience of riblet surface, and it is found that a maximum drag reduction rate of 8% is obtained with a V-shaped riblet surface. Recently, the friction drag mechanism with a riblet surface becomes clear by a detailed experiment using 3-D particle tracking velocimetry (3-D PTV) (Suzuki and Kasagi, 1994) and direct numerical simulation (DNS) (Choi *et al.*, 1993).

A dolphin also swims as fast as 40 knots per hour at maximum, however, it is well-known as "Grey's paradox" that its muscle is not strong enough for swimming in such a fast speed (Gray, 1936). Therefore, it is expected that flexible skin of a dolphin (compliant surface) plays a key role in controlling the surrounding fluid. Research works of compliant surface were started by the experiment of Kramer (1960), and it has been reported that a compliant surface has the effect of transition delay and friction drag reduction.

Many experiments and numerical calculations with Orr-Sommerfeld equation have been progressed, investigating the transition delay of compliant surface, (e.g. Bushnell *et al.*, 1977; Riley *et al.*, 1988; Gad-el-Hak, 1996). Carpenter and Garrad (1985) modeled a compliant surface to an elastic plate supported by an array of springs, and found that the critical Reynolds number is increased. They suggested that there exists an optimal combination of the material property of compliant surface for turbulent transition delay.

On the other hand, mode than 20% of friction drag reduction is reported by Kramer (1960) and Chu and Blick (1969). However, the reliability of these results are open to question in respect of the accuracy of the measurement. No detailed data has been obtained, since there are many difficulties in the experiment with compliant surface, that the material property is quite sensitive to the change of the environment of the experimental facility, as well as the difficulty of the measurement over a moving boundary.

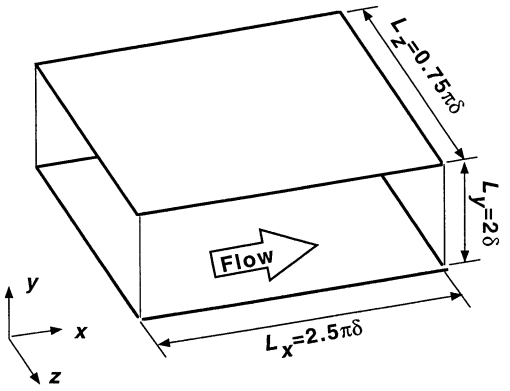

Figure 1: Flow geometry and coordinate system.

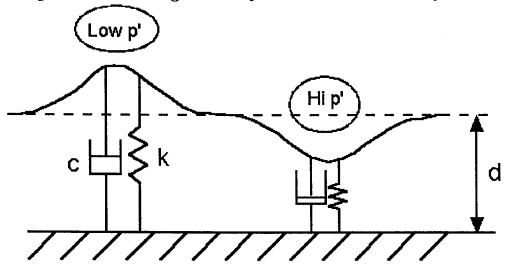

Figure 2: A schematic of the model for a compliant surface.

The objective of the present study is to obtain detailed data of turbulent flow field over deforming compliant surface with the aid of DNS. Effect of friction drag reduction with complaint surface is evaluated, and the mechanism of the drag reduction is investigated. It is also desired to obtain an optimal material property of a compliant surface for drag reduction.

NUMERICAL PROCEDURE

The flow geometry and the coordinate system are shown in Fig. 1. The governing equations are the incompressive Navier-Stokes equations and the continuity equation. The wall deformation is described with a boundary-fitted coordinate system for moving boundary. Periodic boundary conditions are employed in the streamwise ($x-$) and the spanwise ($z-$) directions, while non-slip boundary condition is imposed on the top and bottom deformable walls.

A modified Crank-Nicolson type fractional-step method (Choi and Moin, 1994) is used for the time advancement, while a second-order finite difference scheme is employed for the spatial discretization of both flow variables and metrics on a staggered mesh (Mito and Kasagi, 1998). The pressure Poisson equation is solved with the multi-grid method (Demuren and Ibraheem, 1998). Successive over relaxation (SOR) method is adopted in the finer and the coarser meshes.

The size of the computational volume is $2.5\pi\delta$ in the streamwise direction and $0.75\pi\delta$ in the spanwise direction (where, δ is the channel half width), which correspond to about 1180 and 360 viscous length units, respectively. It is about 2.5 and 3.6 times larger than the so-called minimal flow unit (Jiménez and Moin, 1991). Hereafter, all the parameters with a superscript + represent quantities non-dimensionalized by the friction velocity u_τ in the plane channel flow and the kinematic viscosity ν.

The number of grid points is 96, 97 and 96 in the $x-, y-$ and $z-$directions, respectively. Uniform meshes are used in the $x-$ and $z-$directions with spacings $\triangle x^+ = 12$ and $\triangle z^+ = 3.7$. A non-uniform mesh with a hyperbolic tangent distribution is used in the $y-$direction. The first mesh point away from the wall is given at $y^+ = 0.25$.

The computational time step is $0.33\nu/u_\tau^2$. The simulation is performed under the constant flow rate condition throughout the present study. The Reynolds number based on the bulk mean velocity U_b and the channel width 2δ is 4600 (about 150 based on u_τ and δ for the plane turbulent channel flow). An instantaneous flow field of a fully-developed turbulent channel flow was used for the initial condition.

MODELING OF COMPLIANT SURFACE

In the first stage of the present study, material property of the compliant surface is assumed to be isotropic. Carpenter and Morris (1990) found that the anisotropy of the deformation of compliant surface contributes towards the stabilization of Traveling-Wave Flutter (TWF). However, a simple model of a compliant surface is used in the present study to investigate the influence of the deformation of compliant surface on the turbulent coherent structure. Each grid point on the compliant wall is assumed to move only in $y-$direction, and the deformation of the compliant surface is modeled in a spring, mass, and damper system (Fig. 1), The wall deformation is determined as follows;

$$m\frac{\partial^2 y_w}{\partial t^2} + c\frac{\partial y_w}{\partial t} + k y_w = \Delta x \Delta z \left(-p'_w + T_x \frac{\partial^2 y_w}{\partial x^2} + T_z \frac{\partial^2 y_w}{\partial z^2} \right), \quad (1)$$

where, m is the mass of compliant surface for

one calculation grid volume, and is determined as $m \equiv \rho_c \cdot \Delta x \cdot \Delta z \cdot d$ (ρ_c and d are the density and the thickness of th compliant surface, respectively). And, c and k are damping parameter and spring stiffness, p'_w denotes wall pressure fluctuation, and T_x and T_z are tensions employed in the streamwise and the spanwise directions, respectively.

It is shown that many parameters are necessary to be determined in Eq. (1). The material properties of the compliant surface used in the present study are $\delta = 0.04[m]$, $\nu = 10^{-6}[m^2/s]$, $d = 28[mm]$ and fluid density $\rho_f = 10^3[kg/m^3]$, and are set to be constant. In the present study, the tensions employed in horizontal directions T_x and T_z are neglected for the simplicity. And the remaining parameters c and k are under investigation. Note that the spring stiffness ω_0 is related to Young's modulus Y of the compliant surface by the following equation;

$$\omega_0 = \sqrt{\frac{k}{m}} = \sqrt{\frac{Y\Delta x\Delta z/d}{\rho_c \Delta x \Delta z}} = \frac{1}{d}\sqrt{\frac{Y}{\rho_c}}. \quad (2)$$

The Young's modulus of elastic rubber is of the order of $1[MPa]$, and that of human skin is $150[MPa]$. In the present study, the Young's modulus (the spring stiffness) is determined to be relatively small, so that the deformation of the compliant surface is sufficiently large to investigate the influence of the deformation on the turbulent coherent structures. Here, $Y = 92.75[Pa](k = 0.011[kg/s^2])$ is adopted. Gad-el-Hak *et al.*(1984) used a compliant surface, which is a mixture of polyvinyl chloride resin (PVC) and dioctyl phthalate, with Young's modulus of $5 \sim 12,500[Pa]$ depending on the mixture rate. Therefore, the assumed material of the compliant surface used in the present study is not impractical. For the damping coefficient, Case1: $c = 0$, Case2: $c = 4.0 \times 10^{-4}[kg/s]$, and Case3: $c = 1.6 \times 10^{-3}[kg/s]$ are tested.

RESULTS AND DISCUSSIONS

Time trace of the volume-averaged streamwise pressure gradient, which is normalized by that in the plane channel flow is shown in Fig. 3. Note that the form drag of the deformable walls are found to be negligible, so the friction and total drags are employed synonymously in the present study. In Case 1, both the friction drag and turbulent kinetic energy are increased from $t^+ = 300$, and the calculation is diverged since the grid resolution becomes insufficient to analyze the turbulence. On the other hand, in Cases 2 and 3, in which proper damping coefficient is adopted, the friction drag is decreased slightly compared to that of the plane channel flow. The mean reduction rate of friction drag in Cases 2 and 3 during the period of $t^+ = 0 \sim 1000$ are 1.7% and 2.7%, respectively.

When the compliant surface is applied to the turbulence control device, the drag reduction rate obtained in Cases 2 and 3 is not practical with the production cost being taken into account. However, it is found that the drag reduction is possible by the compliant surface, which is deformed passively by the pressure fluctuation of the flow. And it is expected that more drag reduction is obtained by optimizing the material property of the compliant surface.

Figure 4 shows the time trace of the rms

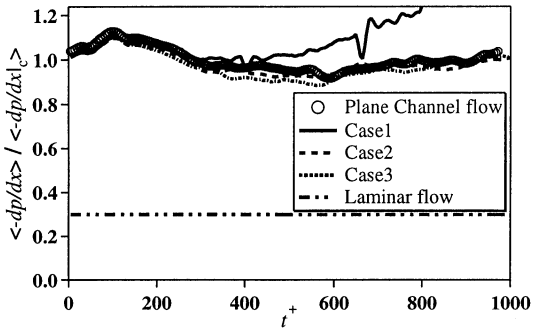

Figure 3: Time trace of the normalized mean pressure gradient.

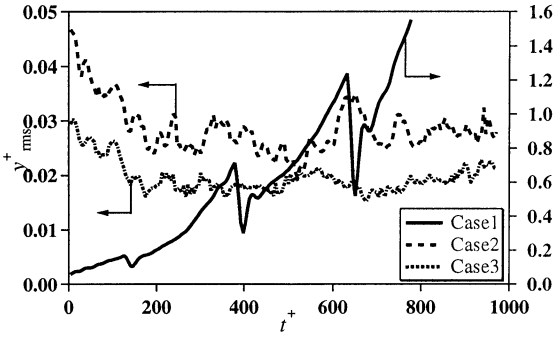

Figure 4: Time trace of the rms value of wall displacement.

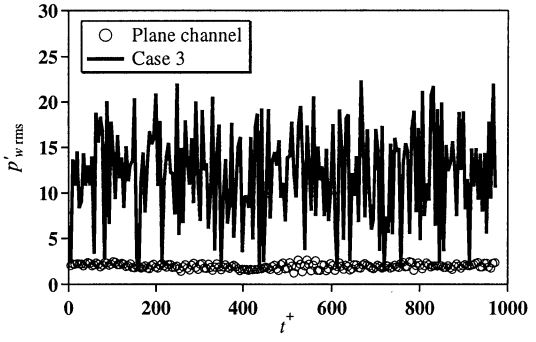

Figure 5: Time trace of the rms value of wall pressure fluctuation.

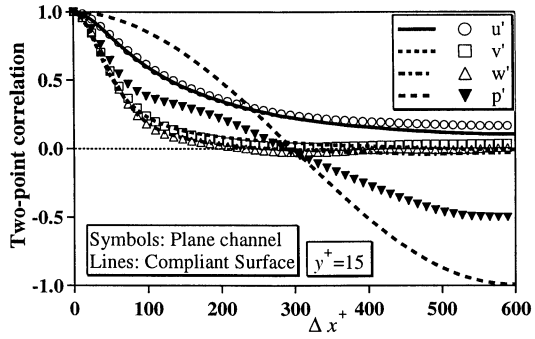

Figure 6: Two-point correlation of velocity and pressure fluctuations in streamwise direction at $y^+ = 15$.

(a)

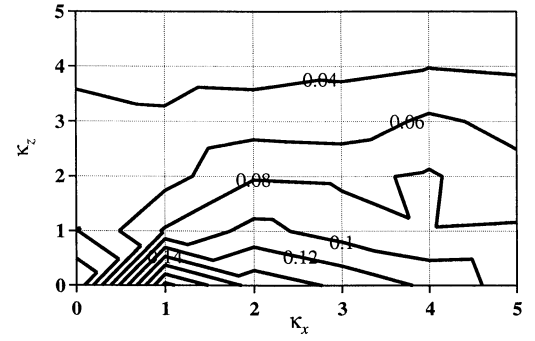

(b)

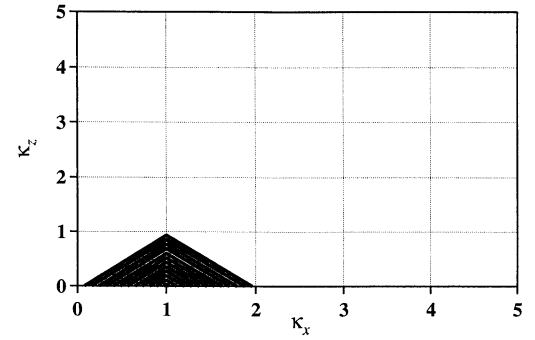

Figure 7: Two-dimensional spectrum. (a) Wall displacement y_w^+, (b) Wall velocity v_w^+

value of the wall displacement y_w^+. In Case 1, wall displacement becomes excessively large by resonating with the pressure field. On the other hand, wall displacements in Cases 2 and 3 remain definite values in the period of $t^+ > 200$, by the damping of the compliant surface. The values are quite small and are of the order of $y_{w\,rms}^+ \sim 0.03$. Although it is not shown here, the rms value of wall velocity $v_{w\,rms}^+$ is approximately 0.25, and is quite small value.

The time traces of the rms value of wall pressure fluctuations $p_{w\,rms}^+$ of the plane channel flow and Case 3 are shown in Fig. 5. Although the wall velocity $v_{w\,rms}^+$ is quite small, wall

(a)

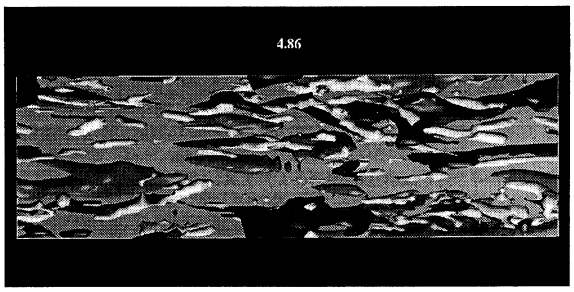

(b)

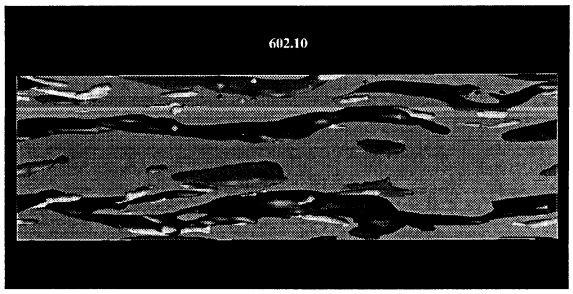

Figure 8: Instantaneous flow field of plane channel flow. (a) $t^+ = 4.86$, (b) $t^+ = 602.1$. Blue: $u'^+ = -3.5$, Red: $u'^+ = 3.5$, White: $II'^+ = -0.03$.

(a)

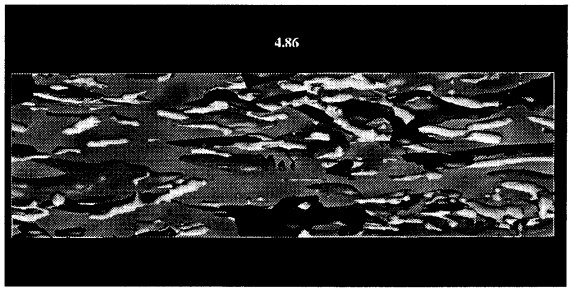

(b)

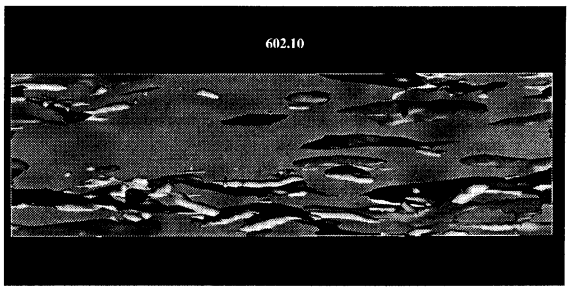

Figure 9: Instantaneous flow field of Case 3. For caption, see Fig. 8.

pressure fluctuation in Case 3 is drastically increased than that in the plane channel flow. Therefore it is expected that the small deformation of the compliant surface can change turbulence coherent structures drastically, by optimizing the material parameters.

Figure 6 shows the profiles of two-point correlation of velocity and pressure fluctuations

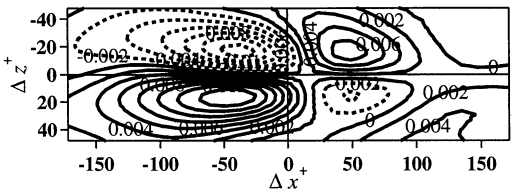

Figure 10: Contours of the streamwise vorticity at $y^+ = 15$ near low-pressure region.

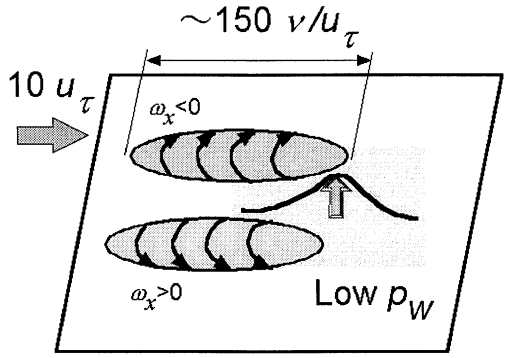

Figure 11: A schematic of flow field near low-pressure region.

in $x-$ direction for the plane channel flow and Case 3. Although there are little difference in the velocity field, the pressure field differs significantly. The two-point correlation of the pressure fluctuation in the spanwise direction is almost unity over the whole spanwise length of the calculation domain (not shown here). Therefore, it is expected that quite large scale of the pressure field becomes dominant over a deformable compliant surface.

Two-dimensional $(x - z)$ spectrum of the wall displacement y_w and velocity v_w in Case 3 are shown in Fig. 7. The peak is observed at $(\kappa_x, \kappa_z) = (1,0)$ for both y_w and v_w, which shows that the typical displacement and the velocity have a scales of approximately 600 and 360 viscous lengths in the streamwise and the spanwise directions, respectively. And, the strength of the wall displacement and the velocity of which wave number over $(\kappa_x, \kappa_z) = (5,5)$, is quite small. Thus, the deformation of the compliant surface is relatively large. This fact is expected to have close relation with the large scale of the pressure fluctuation at $y^+ = 15$ as shown in Fig 6, however, it is unclear yet why the large scale of the pressure fluctuation becomes dominant over the compliant surface, and is a future subject of our study.

Figure 8 shows the top views of instantaneous flow fields of the plane channel flow. Flow direction is left to right. Gray and black contours are high- and low-speed streaks, respectively, while white shows the vortical structure ($II'^+ = -0.03$, II' is the second invariant of the deformation tensor) (Chong *et al.*, 1990; Kasagi *et al.*, 1995). Vortical structures are mostly observed at the downstream edge of the meandering low-speed streaks (Jeong *et al.*, 1997; Endo *et al.*, 2000). And, it is observed that regeneration of the vortical structure is occurred continuously, by activating the meandering of the streaks with its rotation.

Figure 9 shows the top view of the instantaneous flow field of Case 3. The wall shading describes the wall displacement y_w. Since remarkable drag reduction is not obtained in the present calculation, there observed little qualitative difference in vortical and streaky structures. However, the contours of the high- and low-speed streaks are found to be slightly small. This fact corresponds to the slight decrease of the two-point correlation of the streamwise velocity fluctuation in the streamwise direction at $y^+ = 15$ shown in Fig. 5. The typical shape of wall deformation is a wave of which the deformation is homogeneous in the spanwise direction. This shape is qualitatively same as that visualized in the experiments of Hansen *et al.*(1980) and Gad-el-Hak (1984).

In order to examine flow characteristics associated with high- and low- pressure region on the wall, a conditional average of a plane channel flow is made, given the condition of the signs of $p_w'^+$ on the wall. A threshold of $|p_w'^+| = 2.0$ is employed to extract strong events only. Figure 10 shows contours of the conditionally averaged streamwise vorticity $< \omega_x^+ >$ at $y^+ = 15$ near low-pressure region. The detection point is at the center of the figure. The wall-normal velocity component above high- and low-pressure on the wall is negative and positive, which indicates that there occurs sweep (Q4) and ejection (Q2) event, respectively. When there is no phase delay in the spring, mass, and damper system (Fig. 2), the compliant wall may have positive wall-normal velocity near low-pressure region, where ejection event occurs as schematically shown in Fig. 11. And negative wall-normal velocity is occured near sweep event. It is expected that the wall velocity would strengthen the rotation of the vortices accompanied by the ejection and sweep events, and contributes to increase Reynolds shear stress. Therefore, it would be necessary that the spring, mass, and damper system, which is a model of the compliant surface, have phase delay from the wall pressure

fluctuation, to have drag reduction mechanism.

CONCLUSIONS

DNS of turbulent channel flow with compliant walls, which is deformed passively by wall pressure fluctuation, was made to evaluate friction drag reduction effect. Compliant surface is modeled to a spring, mass and damper system.

The typical shape of the deformation is a wave of which a period in the streamwise direction is approximately 1200 viscous length units. And approximately $2 \sim 3\%$ of drag reduction is observed in the present study.

Although there observed little influence on the velocity field, the pressure field is drastically affected. Therefore, it is expected that a compliant wall is possible which impacts on the velocity field, when the material property of the compliant surface is optimized.

From the conditionally averaged flow field, the ejection and sweep events are occured upstream of high- and low-pressure on the wall. Therefore, it is supposed that a phase delay of the spring, mass, and damper system is necessary to suppress the rotation of the quasi-streamwise vortical structure accompanied by ejection and sweep events.

REFERENCES

Bushnell, D. M., Hefner, J. N. and Ash, R. L., 1977, "Effect of Compliant Wall Motion on Turbulent Boundary Layers," *Phys. Fluids*, Vol. 20, pp. S31-S48.

Carpenter, P. W. and Garrad, A. D., 1985, "The Hydrodynamic Stability of Flow over Kramer-type Compliant Surfaces. Part 1. Tollmien-Schlichting Instability," *J. Fluid Mech.*, Vol. 155., pp. 465-510.

Carpenter, P. W. and Morris, P. J., 1990, "The Effect of Anisotropic Wall Compliance on Boundary-Layer Stability and Transition," *J. Fluid Mech.*, Vol. 218, pp. 171-223.

Choi, H., Moin, P., and Kim, J., 1993, "Direct numerical simulation of turbulent flow over riblets," *J. Fluid Mech.*, Vol. 255, pp. 503-539.

Choi, H., and Moin, P., 1994, "Effects of the computational time step on numerical solutions of turbulent flow," *J. Comput. Phys.*, Vol. 113, pp. 1-4.

Chong, M. S., Perry, A. E. and Cantwell, B. J., 1990, "A General Classification of Three-Dimensional Flow Fields," *Phys. Fluids A*, Vol. 2, No. 5, pp. 765-777.

Chu, H. H. and Blick, E. F., 1969, "Compliant Surface Drag as a Function of Speed," *J. Spacecraft and Rockets*, Vol. 6, pp. 763-764.

Demuren, A.O., and Ibraheem, S.O., 1998, "Multigrid method for the Euler and Navier-Stokes equations," *AIAA J.*, Vol. 36, pp. 31-37.

Endo, T., Kasagi, N. and Suzuki, Y., 2000, "Feedback Control of Wall Turbulence with Wall Deformation," *Int. J. Heat & Fluid Flow*, Vol. 21, pp. 568-575.

Gad-el-Hak, M., 1996, "Compliant Coatings," *Appl. Mech. Rev.*, Vol. 49, No. 10, pp. S147-S157.

Gad-el-Hak, M., Blackbwelder, R. F. and Riley, J. J., 1984, "On the Interaction of Compliant Coatings with Boundary-Layer Flows," *J. Fluid Mech.*, Vol. 140, pp. 257-280.

Gray, J., 1936, "Studies in Animal Locomotion. VI The Propulsive Powers of the Dolphin," *J. Exp. Biology*, Vol. 50, pp. 233-255.

Hansen, R. J., Hunston, D. L., Ni, C. C., Reischman, N. M. and Hoyt, J. W., 1980, "Hydrodynamic Drag and Surface Deformations Generated by Liquid Flows Over Flexible Surfaces," In *Viscous Flow Drag Reduction*, Hough, G. R., ed., AIAA, pp. 439-452.

Jiménez, J., and Moin, P., 1991, "The minimal flow unit in near-wall turbulence," *J. Fluid Mech.*, Vol. 225, pp. 213-240.

Jeong, J., Hussain, F., Schoppa, W., and Kim, J., 1997, "Coherent structures near the wall in a turbulent channel flow," *J. Fluid Mech.*, Vol. 332, pp. 185-214.

Kasagi, N., Sumitani, Y., Suzuki, Y., and Iida, O., 1995, "Kinematics of the quasi-coherent vortical structure in near-wall turbulence," *Int. J. Heat & Fluid Flow*, Vol. 16, pp. 2-10.

Kramer, M. O., 1960, "Boundary Layer Stabilization by Distributed Damping," *Nav. Eng. J.*, Vol. 72, pp. 25-33.

Mito, Y., and Kasagi, N., 1998, "DNS study of turbulence modification with streamwise-uniform sinusoidal wall-oscillation," *Int. J. Heat & Fluid Flow*, Vol 19, pp. 470-481.

Riley, J. J., Gad-el-Hak, M. and Metcalfe, R. W., 1988, "Compliant Coatings," *Annu. Rev. Fluid Mech.*, Vol. 20, pp. 393-420.

Suzuki, Y. and Kasagi, N., 1994, "Turbulent Drag Reduction Mechanism Above a Riblet Surface," *AIAA. J.*, Vol. 32, No. 9, pp. 1781-1790.

Walsh, M. J., 1982, "Turbulent Boundary Layer Drag Reduction Using Riblets," AIAA Paper 82-0169.